Coastal Dynamics 2017
Paper No. 218

PERFORMANCE OF A TILT CURRENT METER IN THE SURF ZONE

Asger Bendix Hansen[1], Stefan Carstensen[1], Drude Fritzbøger Christensen[2] and Troels Aagaard[2]

Abstract

Tilt Current Meters (TCM's) are relatively simple and inexpensive instruments for measuring currents in rivers and in the sea. Their low cost and easy deployment means that a relatively large number of TCM's can be deployed compared to more conventional current meters such as Acoustic Doppler Velocimeters (ADV's) or Acoustic Doppler Current Profiler (ADCP's). Although, the accuracy of the individual measurements may not be as good as conventional current meters, the possibility of deploying many instruments is a great advantage when studying spatial variations in flows. This is especially the case when data is later used for comparison with numerical models whose results are also associated with considerable uncertainty. Previous studies have mainly considered steady current or tidal flows in which velocities were relatively low and the importance of waves limited. The presence of waves adds a number of important challenges to the measurements as the hydrodynamic forcing changes and the oscillations of the TCM cannot necessarily be averaged out as for a steady current. This study addresses some of these challenges by analyzing the performance of a TCM in the surf zone where wave orbital motion is dominant.

Key words: coastal hydrodynamics, surf zone, observational techniques

1. Introduction

In recent years, the use of tilt current meters (TCMs) as a method for measuring flow speeds in the sea has received renewed attention. With the emergence of low cost micro-electro-mechanical (MEMS) accelerometers and microcontrollers it has become possible to construct a TCM at costs which are orders of magnitude smaller than the conventional flow meters which are otherwise used, e.g. Electro Magnetic Current Meters (EMCM), Acoustic Doppler Velocimeters (ADV) and Acoustic Doppler Current Profilers (ADCP). Although the quality of the flow measurement with a TCM cannot compete with the conventional methods this may be an acceptable trade-off in cases where spatial variations in the flow field are of interest. This is especially the case when measurements are intended for comparison with numerical modelling, the outputs of which often have a larger uncertainty than the field measurements.

Figurski et al. (2011), Lowell et al. (2015), Marchant et al. (2014), and Radermacher et al. (2015) have all recently studied the performance of TCM's in different coastal flows. The TCM's used in these studies vary in size and shape (typically spherical or cylindrical) but the flows considered have mainly been tidal flows with current speeds smaller than 1 m/s. One exception is Figurski et al. (2011) who used a TCM to estimate wave conditions by looking at the standard deviation of the TCM tilt. Results from previous studies show that TCM's can deliver quite good accuracies (0.05 m/s, Marchant et al., 2014 or 2% Lowe et al., 2015).

The promising results observed in these studies encourage further development of the technique so that it might be applied in a wide variety of flow conditions. More specifically, we are interested in developing the use of TCM's in the surf zone. The presence of waves adds a number of important challenges to the measurements as the hydrodynamic forcing changes and motion of the TCM may affect the measurement. Some of these issues were addressed by (Hansen and Carstensen, 2017) who investigated the behavior of generic TCM's in waves theoretically and in a series of laboratory experiments. The generic TCM's

[1] Department of Mechanical Engineering, Technical University of Denmark, Niels Koppels Alle, Building 403, DK-2800 Kgs. Lyngby, Denmark. asbha@mek.dtu.dk, scar@mek.dtu.dk
[2] Institute of Geosciences and Natural Resources, University of Copenhagen, Øster Voldgade 10, DK-1350 Copenhagen K., Denmark. dc@ign.ku.dk , taa@ign.ku.dk

covered a spherical floater and various cylindrical floaters with hemispherical end caps. Based on this a recommendation was given for dimensioning a TCM suitable for use in the surf zone.

An opportunity to do an ad-hoc field test arose during the study reported by Hansen and Carstensen (2017). This paper presents the result of this field test. In the field test, the measured flow velocity of one of the TCM's tested by Hansen and Carstensen (2017) was compared with those made by a nearby positioned ADV.

2. Measuring principle

A TCM (Figure 1) estimates flow speed, U, from measured tilt angle, θ, given a known response curve. The generic tilt current meter shown in Figure 1 has a cylindrical flotation body of length l with circular cross-section and spherical end caps. The pivot point combined with the stiff tether limits the degrees of freedom of the floatation body to pitch and roll.

Two issues have to be addressed in order to establish a theoretical response curve for an unsteady flow (Hansen and Carstensen, 2017). First, the in-line hydrodynamic load has two contributions (drag and inertia forces). Secondly, the natural frequency of the TCM could coincide with frequencies in the flow causing resonance.

Regarding the in-line hydrodynamic load, the relative importance of the drag force and inertia force are described by the Keulegan-Carpenter number

$$KC = \frac{U_m T}{D} \tag{1}$$

where U_m is the maximum wave orbital velocity, $T = 1/f_w$ is the wave period, f_w is the wave frequency and D the diameter of the body. The drag force becomes increasingly important as the KC number is increased. For example, a fixed cylinder may be considered drag-dominated for KC numbers larger than 20 – 30 (Sumer and Fredsøe, 2006). This suggests that inertia may be neglected as long as the TCM is sufficiently small.

The natural frequency of the TCM may be estimated by considering the TCM as an immersed pendulum damped by viscous and inertia forces (Sumer and Fredsøe, 2006). Hence, the natural frequency can be expressed as

$$f_n = \frac{1}{2\pi}\sqrt{\frac{F_B}{L_m\left(m+m'\right)}} \tag{2}$$

where F_B is the net submerged weight (equation 4), m is the mass, $m' = \rho C_m V$ is the hydrodynamic mass in which C_m (= ½ for a sphere, hence $½ \leq C_m < 1$ for $l \geq 0$ in an ideal fluid) is the hydrodynamic mass coefficient of the floatation body, and L_m is the distance from the pivot point to the center of mass of the floatation body (see Figure 1). Assuming a uniform mass distribution in the floater this distance is $L_m = L + ½(D + l)$, where L is the tether length and D is the diameter of the floater. The natural frequency of the TCM should be sufficiently larger than the expected wave frequencies in order to avoid resonance and a frequency dependent response curve. This can be achieved by carefully choosing the dimensions of the TCM.

With this in mind, the theoretical response curve can be determined by considering the force balance in the angular direction (see Figure 1) between the drag force, $F_{D,\theta}$, and the net submerged weight

$$F_B \sin(\theta) = F_{D,\theta} \tag{3}$$

The net submerged weight can be written

$$F_B = g(\rho V - m) \tag{4}$$

where ρgV is the buoyancy force on the floatation body, ρ is the density of water, g is gravitational acceleration, and V is the volume of the body.

The drag force in the angular direction can be expressed using the cross-flow principle (Sumer and Fredsøe, 2006) by

$$F_{D,\theta} = \frac{1}{2}\rho C_D A U_\theta^2 = \frac{1}{2}\rho C_D A \cos^2(\theta) U^2 \tag{5}$$

where C_D is the drag coefficient, A is the frontal projection area of the floatation body and $U_\theta = U \cdot \cos(\theta)$ is the velocity normal to the floatation body axis. Ideally, the drag coefficient assumes an approximately constant value (Hansen and Carstensen, 2017). This can be achieved by carefully choosing the dimensions of the TCM.

Inserting the expression for the two forces (Equations 4 and 5) into equation (3) and solving for U gives

$$U = k\sqrt{\frac{\tan(\theta)}{\cos(\theta)}} \tag{6}$$

where k is a function of the TCM properties (essentially mass and diameter) as well as the drag coefficient

$$k = \sqrt{\frac{2g(\rho V - m)}{\rho C_D A}} \tag{7}$$

Equation (6) and (7) can be used to obtain the flow speed, U, from the tilt angle, θ. The flow direction is given by the tilt direction, φ. The flow speed and direction can then subsequently be converted into the horizontal velocity components (u and v) of the flow.

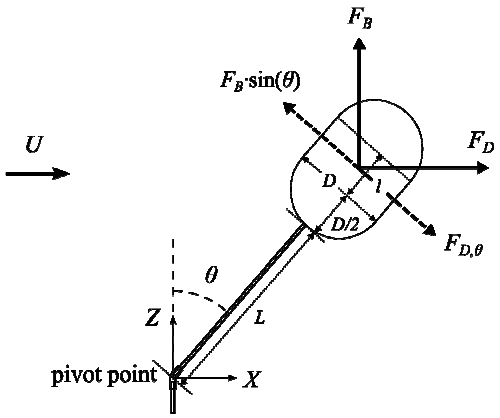

Figure 1. Definition sketch of a generic tilt current meter with a stiff tether of length L and a pivot point that only allows pitch, β, and roll motion, α. The floatation body is a circular cylinder having diameter D and length l with hemispherical end caps. Flow speed, U, is derived from the tilt angle, θ.

3. Technical specifications

The left panel in figure 2 shows the prototype TCM and Table 1 lists its dimensions.

The floatation body of the TCM is tethered with a rigid carbon fiber tube to a watertight box through a flexible rubber tube (the pivot point). Accelerometer, gyroscope and magnetometer (9-DOF) are mounted inside the floatation body. Electrical wires run inside the tether and connect the sensors to a microcontroller (Arduino Pro Mini) located in the watertight box along with a real time clock, SD-card for data logging and batteries. An absolute pressure transducer is mounted in the bottom of the watertight box and is recorded with the same microcontroller ensuring synchronous measurement of tilt and direction of the TCM as well as pressure. The water surface elevation can be estimated from the measured pressure. Surface elevation is important, as the TCM has to be submerged in order to give reliable data using equation 6.

Equation 6 is the so-called response curve for the TCM. It can be used to convert measured tilt angle to an estimate for the flow speed. The coefficient k in equation 6 equals 0.42 for the present TCM. The right panel in Figure 2 shows the response curve for this TCM. Also included in the figure is calibration data for both steady current and waves. The calibration data was measured in dedicated laboratory tests at the hydraulic laboratory at the Technical University of Denmark. Details of these laboratory tests are given in Hansen and Carstensen (2017).

The orientation of the floatation body in a stationary position can be determined from the measured accelerations with respect to the gravitational field. The z-axis of the accelerometer is positioned in-line with the tether with the positive direction upwards. This means that the accelerometer measures (a_x, a_y, a_z) = (0,0,-1g) when the TCM is in the vertical position. Here a_x, a_y and a_z are the accelerations in the local coordinate system of the floatation body.

Since the TCM is limited to roll and pitch motion (orthogonal to the accelerometers z-axis) then there are no inertial accelerations and the only contribution to a_z is the gravitational acceleration, g. Hence, tilt angle of the TCM can be easily determined also in a non-stationary state by

$$\theta = \cos^{-1}\left(\frac{a_z}{g}\right) \tag{8}$$

The tilt direction, φ, of the floatation body in the stationary position can likewise be determined with respect to the gravitational field.

$$\varphi = \cos^{-1}\left(\frac{a_x}{\sqrt{a_x^2 + a_y^2}}\right) \quad \text{or} \quad \varphi = \sin^{-1}\left(\frac{a_y}{\sqrt{a_x^2 + a_y^2}}\right) \tag{9}$$

Using this relationship also in the non-stationary state result in errors resulting from e.g. inertial accelerations in a_x and a_y. It is possible to compensate for this error by combining the acceleration readings with the gyroscope reading. The two common methods for applying this compensation are known as complementary filter and Kalman filter. Applying such filters would remove much of the error caused by inertial motion of the TCM as well as electrical noise. This type of filtering has not been performed in the present post-processing.

Equation (6) and (7) can be used to obtain the flow speed, U, from the tilt angle, θ. The flow direction is given by the tilt direction, φ. The flow speed and direction can then subsequently be converted into the two horizontal velocity components (u and v) of the flow along the X- and Y-axis of the TCM.

$$u = U\frac{a_x}{\sqrt{a_x^2 + a_y^2}} \qquad \text{and} \qquad v = U\frac{a_y}{\sqrt{a_x^2 + a_y^2}} \tag{10}$$

The final step is to use the magnetometer to define these velocities relative to the geographical coordinate system (i.e. as cross-shore and long-shore velocity components).

To achieve a greater accuracy, the response curve may be fitted to the calibration data rather than using equation 6 and 7 (see Hansen and Carstensen, 2017). This was utilized in the present post-processing. Furthermore, in the present treatment of the data, noise on the measurement was removed by filtering the calculated components of flow velocity with a 2Hz low pass filter using a hamming window.

Table 1. Properties of the present tilt current meter.

L [mm]	l [mm]	D [mm]	V [cm^3]	A [cm^3]	m [g]	k	$m^* = m/(\rho V)$	f_n [s^{-1}]
100	50	32	57.4	24.0	28	0.42	0.49	1.06

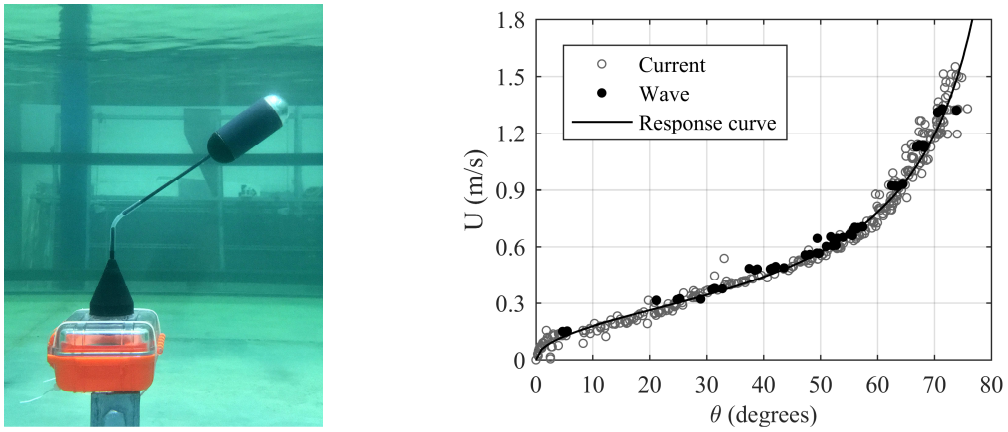

Figure 2. Present tilt current meter. Left: Picture taken in current flume at the hydraulic lab at the Technical University of Denmark (DTU). Right: Response curve (Hansen and Carstensen, 2017).

4. Field experiment

The performance of the prototype TCM in the surf zone was tested in conjunction with the TASTI field experiment (Brinkkemper et. al. 2017) which was carried out in September and October 2016 at Vejers Beach on the Danish North Sea coast. Vejers Beach experiences semidiurnal tides ranging from 0.6 m (neap) to 1.2 m (spring) and has a multiple (3-4) bar system. As part of the experiment, a rig containing three acoustic current meters (SonTek ADVOcean probes) was deployed on the seaward flank of the intertidal bar (Figure 3). One of these ADVs is used as reference to the present TCM measurement. The TCM was deployed at the same cross-shore location, however separated by approximately 1.5 m in the longshore direction from the reference ADV. The TCM was placed at approximately the same height above the bed as the reference ADV.

The ADV measured in periods of 30 minutes every hour with a sampling frequency of 10 Hz. Flow velocities were rotated numerically in order to minimize small tilt errors of the sensors. Instrument noise in velocity time series recorded by acoustic sensors is very common, especially, in the surf zone due to the presence of air bubbles and data points with a signal correlation value lower than an applied threshold of 55 % were replaced by a filtered value obtained from a 0.5 second moving average.

The spatial distance between the TCM and the ADVs did not allow for a direct comparison. For this reason, no attention was given to synchronize the clock on the TCM and the ADV's. Still, the relatively uniform coastal profile suggests that the time series of velocity estimated from the TCM could be compared with the velocity measured by the ADV provided a cross-correlation was first performed. The cross-correlation was performed using the cross-shore velocity component and subsequently applied to the longshore velocity component as well. In this way, comparable time-series of cross-shore and long-shore velocity for both the TCM and the ADV was obtained. The data from the TCM (and pressure sensor) has been organized in a similar way as the ADV data even though the recordings cover the entire deployment period

During the period of the TCM deployment the wave conditions were gentle with a small, long period swell ($H_s \leq 0.6$ m and $T_p \approx 12$ - 13 s) coming from the North West. These conditions meant that waves were breaking at the location of the instruments during part of the tidal cycle. Furthermore, there was an observable longshore current towards the south.

Figure 4 shows the wave spectrum for the highest recorded significant wave height, H_s. This significant wave height was recorded just prior to high tide as shown in figure 5 (grey hatched area). The wave spectrum and tidal variation were calculated based on the estimated surface elevation, which was derived from the pressure recordings using a hydrostatic transfer function.

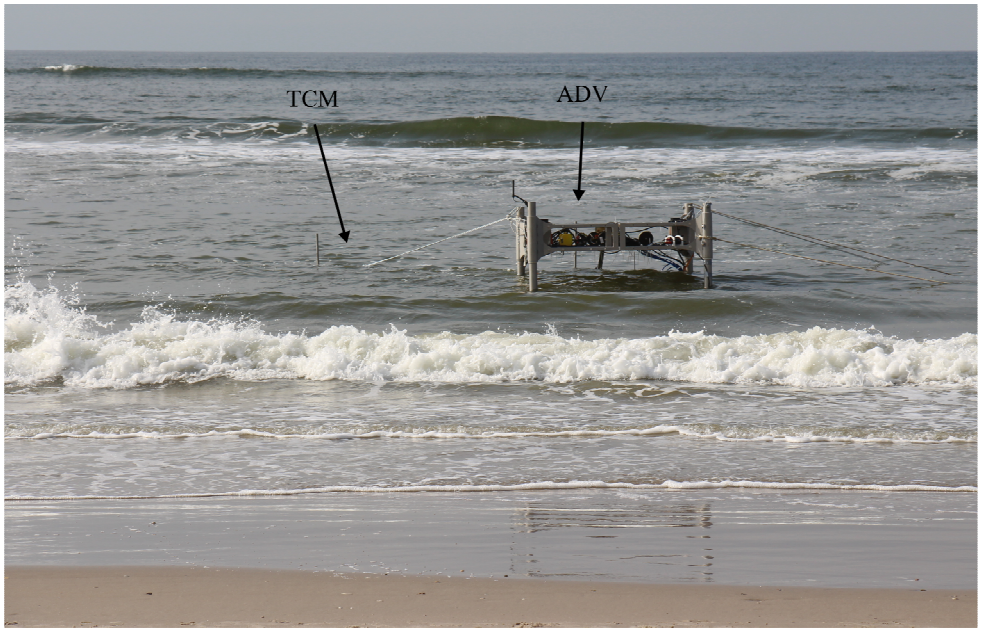

Figure 3. Photo of the field setup at low tide on a calm day

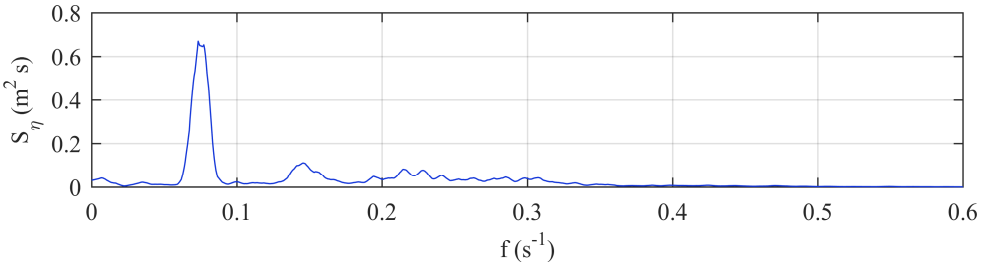

Figure 4. Wave (energy) spectrum on September 21, 2016 between 17:00 and 17:30. H_s = 0.6 m and T_p = 13.3 s.

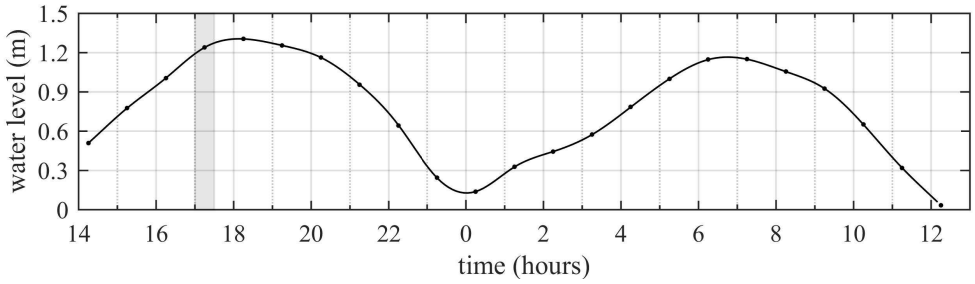

Figure 5. Water level above the pressure sensor showing the tidal variation during the field experiment. The time series start on September 21, 2016 at 14:00. The half-hour period marked in grey is used for detailed comparison between TC M and ADV below. See also wave energy spectrum for this particular interval in figure 4.

5. Results

A time series of flow speed and direction was derived from the accelerometer readings of the TCM as detailed above. First, the accelerometer readings were processed to give tilt angle and direction. Then, the response curve presented in figure 2 was applied to the tilt angle to give the flow speed. Finally, the flow speed and direction was recalculated to cross-shore and long-shore velocity components, u and v, respectively. Due to an issue with the magnetometer in the TCM, the rotation of velocity components from the TCM coordinates to long-/cross-shore direction was done based on the wave direction. The wave direction was determined as the direction in which the variance of the velocity was largest. Comparing the wave direction in the TCM measurements to that in the ADV measurements allowed for the TCM velocities to be rotated to the ADV coordinate system.

Figure 6 shows a part of the 30-minute long cross-shore and long-shore velocity time-series measured by the TCM and the ADV just prior to high tide where the largest significant wave height was recorded. The cross-shore velocity component, u, measured by the TCM is seen to compare well with that measured by the reference ADV. All peaks are present in both time-series although there is a tendency for the peaks in the TCM data to be slightly lower than in the ADV data. This may be due to the low pass filtering at 2 Hz of the TCM data or it could be a sign that the steady current response curve is not valid right at the peak where the flow is highly transient. One thing to notice is that the natural frequency of the TCM is present in the velocity time series. It is particularly clear at e.g. t = 1580 s in the cross-shore velocity signal shown in figure 6.

The long-shore velocity component, v, measured by the TCM is seen to vary rather similar to that measured by the reference ADV. However, it is apparent that there is an offset between the two signals. This offset could be caused by the spatial distance between the two devices or possibly an offset error in the roll angle.

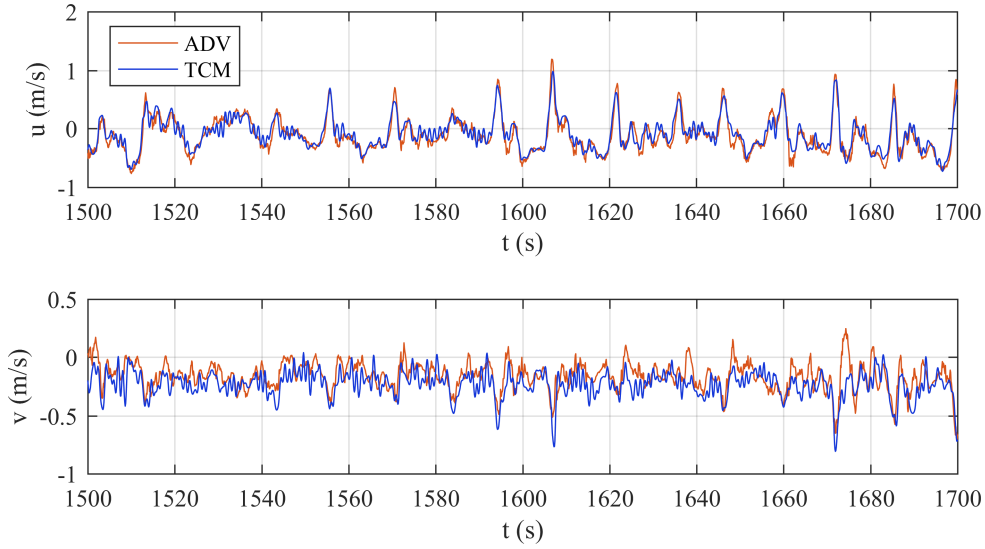

Figure 6. Comparisons of velocity components measured with the TCM and the ADV. Time axis is relative to 17:00 hours on September 21, 2017.

Another way of presenting the cross-shore and long-shore velocity components is as a variance spectrum. The variance spectrum for *u* and *v* measured by TCM and ADV are all given in figure 7. In the range $0 < f < 0.8$ Hz, the variance spectra for both *u* and *v* measured by the TCM and ADV are practically identical at the primary frequencies and quite similar at the higher harmonics. The variance spectrum for the cross-shore velocity is practically identical also at $f = 0$Hz, while the difference in the mean long-shore current seen in figure 6 is naturally present at $f = 0$ Hz in the variance spectrum for *v*. The peak frequency ($f = 0.08$Hz) is clearly visible in the cross-shore velocity and to a lesser extent in the long-shore velocity signal. This indicates that the wave front approaches the coastline at a slight angle which is consistent with the generation of a longshore current. The second and third harmonic of the peak frequency are also noticeable in the spectrum for the long-shore velocity component.

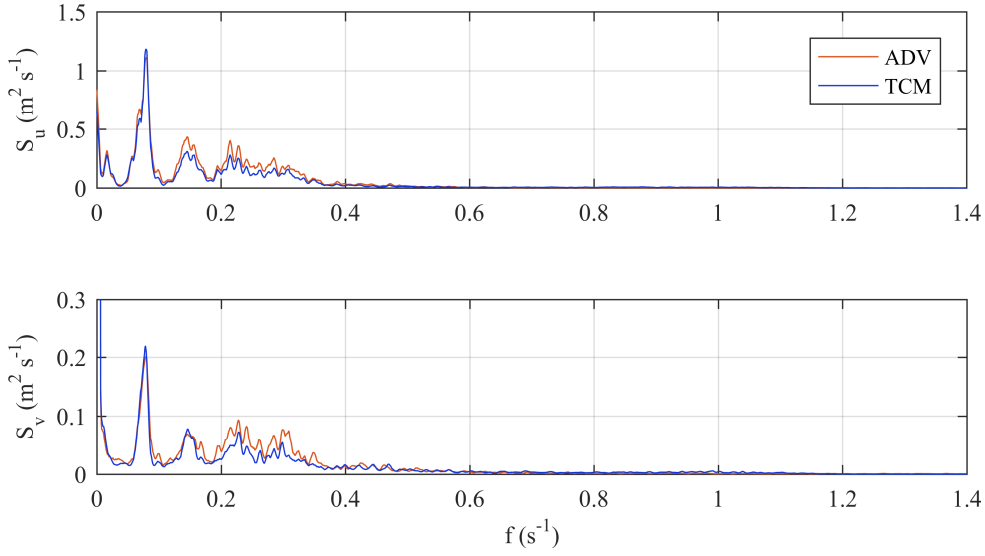

Figure 7. Comparisons of the variance spectrum of the velocity components measured with the TCM and the ADV.

In the range $0.8 < f < 1.2$ Hz there is actually a difference between the variance spectrum for e.g. the cross-shore velocity measured by the TCM and the ADV. Figure 8 shows the variance spectrum for the cross-

shore velocity component on a logarithmic scale. This highlights the difference between the signal measured by the TCM and the ADV in the range $0.8 < f < 1.2$ Hz.

The natural frequency calculated using equation 2 is also shown in figure 8 and is seen to coincide with the range where there is a discrepancy between the cross-shore velocity spectrum measured by the TCM and the reference ADV. Rather than creating a sharp peak in the spectrum, the natural frequency of the TCM is seen to affect a broader range of frequencies. This can be explained by a number of factors: First, equation 2 assumes a small angle approximation to be valid. If this is not the case then the vibration equation becomes non-linear. Secondly, the hydrodynamic mass coefficient may not be a constant but influenced by the flow.

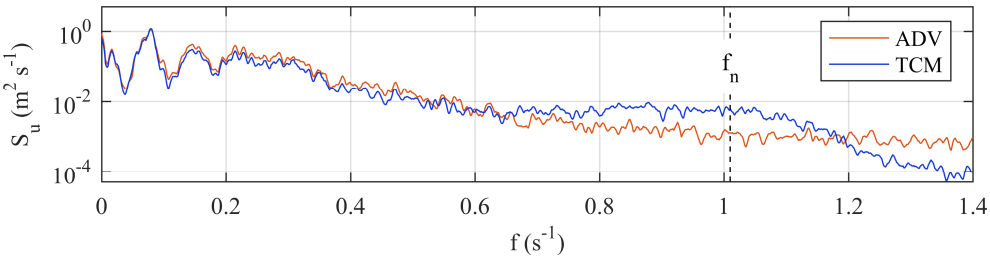

Figure 8. Natural frequency of TCM apparent in the variance spectrum of the cross-shore velocity. Vertical dashed line indicates f_n calculated using equation 2.

Figure 9 presents scatter diagrams of the cross-shore and long-shore velocities measured with the ADV on the horizontal axis and that measured with the TCM on the vertical axis. For the cross-shore velocity, *u*, most of the data points align close to the 1:1 line indicating a good correlation between the ADV and the TCM recordings. This was expected given the time-series comparison presented in figure 6 and the spectrum comparison presented in figure 7.

For the long-shore velocity, *v*, the correlation appears to be not as good as for the cross-shore velocity. This is in agreement with what was observed in the time series plots in figure 6. However, calculating the standard deviation of the TCM velocities from the ADV velocities gives 0.12 m/s for both velocity components.

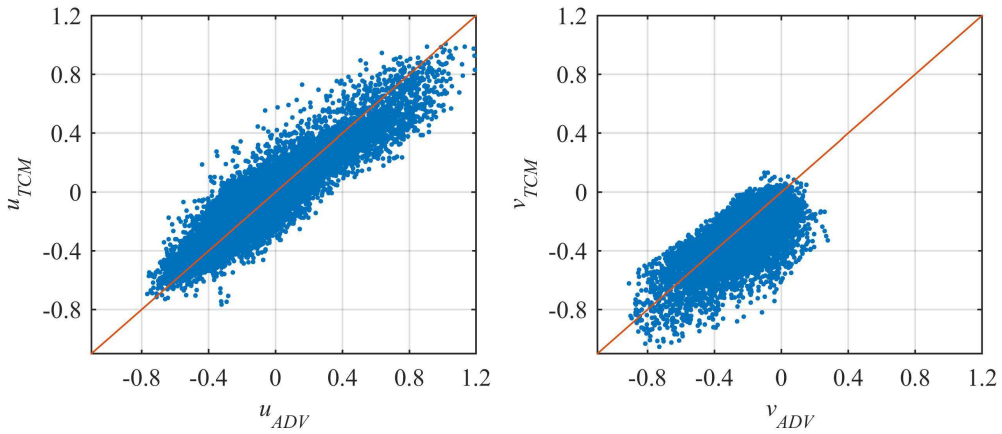

Figure 9. Scatter diagrams of velocities measured with the TCM and the ADV in the cross-shore direction (left panel) and in the long-shore direction (right panel). Red lines represent an exact match. The data set covers the 30-minute burst recorded at 17:00 hours on September 21, 2016.

A summary of the entire data set is shown in figure 10 in the form of a comparison of mean velocities and standard deviations. The standard deviations are related to the significant wave height and can therefore be

taken as a measure of the ability of the TCM to measure the flow related to wave orbital motion, while the mean velocities give an indication of the ability of the TCM to measure wave-averaged velocities.

Figure 10 illustrates that the general observations made previously in the detailed comparisons are valid for the entire data set. That is, the wave motion (represented by the standard deviations) is captured very well by the TCM both in the long-shore and the cross-shore directions. Regarding the wave-averaged flow the TCM gives very good results for the cross-shore component while there is a consistent tendency for the TCM to somewhat overestimate the magnitude of the wave-averaged long-shore current.

While this discrepancy could, in part, be due to the spatial distance between the two sensors it is expected mainly to be due to a certain degree of stiffness in the pivot point of the TCM. Similar behavior of the same TCM was observed by Hansen and Carstensen (2017). A possible explanation is that the forces from the silicone tube which forms the pivot point are not insignificant. It may be that after experiencing an asymmetrical pull over a period of time the tube will show some kind of hysteresis and be more easily turned in one direction than another. Such unwanted behavior could most likely be remedied by improving the construction of the pivot point.

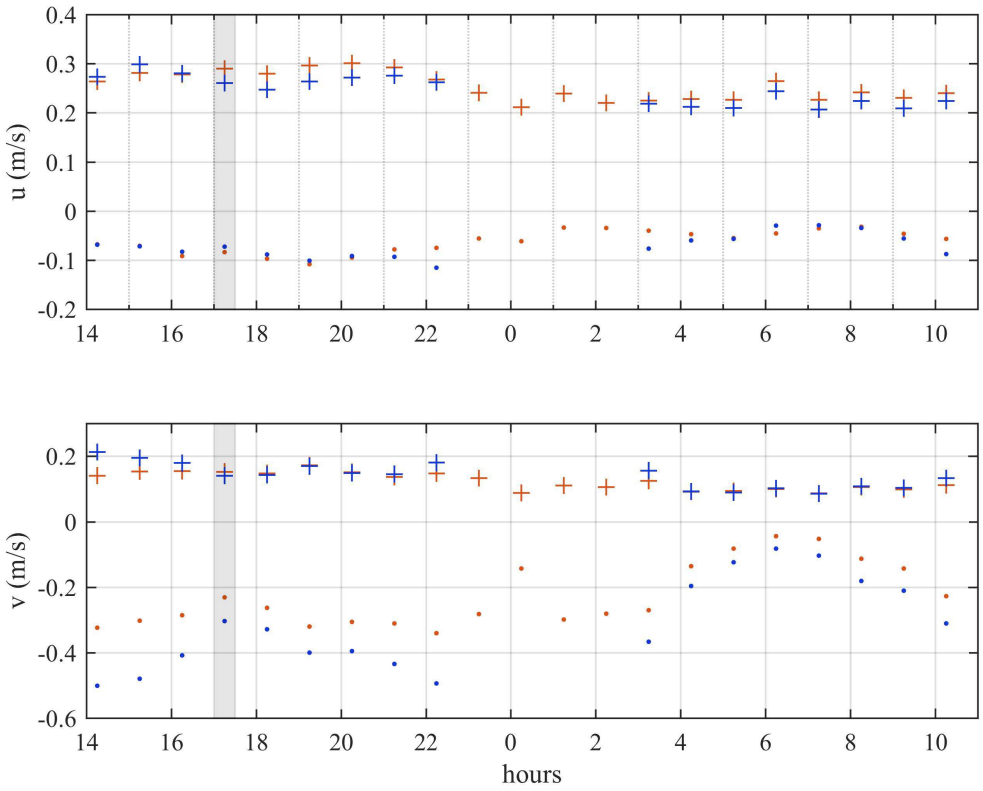

Figure 10. Statistics of the TCM (blue) and ADV (red) flow measurements across the whole test period. '·' mean flow velocities and '+' standard deviation from the mean. Top panel: cross shore velocity, *u*. Bottom panel: Longshore velocity, *v*.

6. Conclusion

The present ad-hoc field test suggests that if properly dimensioned, a TCM is able to provide useful measurements of flow in a wave-dominated environment such as a surf zone. The spatial distance between the TCM and the reference current meter meant that it was not possible to quantify the accuracy of the TCM but in spite of this, good agreement was found between the two measurements. Comparison of both time series and spectra indicate that the TCM captures very well the wave orbital motion both in the cross-

shore and long-shore directions. In the cross-shore direction also the wave averaged velocity was very well captured by the TCM but in the long-shore direction the magnitude of the wave-averaged velocity was overestimated. This overestimation is believed to be due to the construction of the pivot point and can most probably be remedied by improving the design of the pivot point. All in all, the present results suggest that TCMs could be very useful instruments for measuring coastal flows especially when the data is intended for comparison to numerical models. In this case the reduced accuracy of the TCM compared to conventional instruments will often be insignificant but the lower cost of the TCM will allow a much greater spatial resolution which is an advantage when calibrating or validating numerical models.

Acknowledgements

The TASTI field experiment was funded by the Danish Council for Independent Research, grant no DFF-4181-00045. We would like to thank the participants from Utrecht University for good collaboration and discussions.

References

Brinkkemper, J., Christensen, D., Price, T., van Bergeijk, V., Nau, I., van de Wetering, J., Ruessink, G., Ernstsen, V., Aagaard, T., 2017. Surf zone morphodynamics during low-moderate energetic conditions; the TASTI field experiment. *E-proceedings of the Coastal Dynamics conference*, June, 12 – 17, 2017, Helsingør, Denmark.

Figurski, J. D., Malone, D., Lacy, J. R., Denny, M., 2011. An inexpensive instrument for measuring wave exposure and water velocity. Limnology and oceanography: Methods 9, 204–214

Hansen, A. B., Carstensen, S., 2017. Experimental investigation of the performance of tilt current meter in wave-dominated flows. *E-proceedings of the 37th IAHR world congress*, August 13 – 18, 2017, Kuala Lumpur, Malaysia.

Lowell, N.S., Walsh, D.R., Pohlman, J.W., 2015. A comparison of tilt current meters and an acoustic doppler current meter in Vineyard Sound, Massachusetts. *IEEE/OES Eleventh Current, Waves and Turbulence Measurement* 1-7.

Marchant, R., Stevens, T., Choukroun, S., Coombes, G., Santarossa, M., Whinney, J., Ridd, P., 2014. A buoyant tethered sphere for marine current estimation. *Journal of oceanic engineering* 39(1), 2-9.

Radermacher, M., Thackeray, Z., De Schipper, M., Gordon, L., Chrystal, C., Leuci, R., Reniers, A. (2015). Tilt current meter array: Field validation. E-proceedings of the 36th IAHR World Congress, 1-9.

Sumer, B. M., Fredsøe, J., 2006. *Hydrodynamics around cylindrical structures*. World Scientific.